

Continuous direct ohmic heating of liquids

Žitný R. *, Šesták J., Dostál M., Zajíček M.

CTU in Prague, Faculty of Mechanical Engineering
Prague, Czech republic, E-mail: zitny@fsid.cvut.cz

Abstract: An innovated technology of continuous direct ohmic heating of homogeneous liquid foods has been suggested, modeled and tested experimentally. Well known principle of heating is based upon volumetric source of heat due to flow of alternating electrical current through the heated liquid. Our effort was concentrated on the following disadvantage of this technology when applied to continuous heating of highly viscous liquids: non-uniform residence time distribution which causes non-uniform heating of processed liquids and tendency to fouling. Overheating of processed material in the vicinity of electrodes is a severe problem especially for homogeneous liquids, because heterogeneous substances, containing relatively large lumps of solids, exhibit usually a self-cleaning effect. Our design is based on displacement of the overheated boundary layer by the cold liquid flowing from the side channels through perforated electrodes into the heating zone. A simplified analytical solution of laminar Newtonian flow-field in the heater, enabling suitable perforation design, will be presented and compared with the numerical solution by the Fluent program. For verification of theoretical predictions, a semicontinuous experimental apparatus was developed (16 kW, 220 V, 50 Hz, max. temperatures 120 °C). Transparent walls of the heater allowed flow visualization (instantaneous injection of colored tracer) and adjustment of electrodes perforation geometry. Temperature profiles, measured by Pt100 thermometers which were installed directly in the heating zone confirmed, that it is possible to achieve significant improvement of the temperature uniformity.

1. Ohmic heating technology

Continuous direct ohmic heating has been using for many years in different industries and it seems to be promising food processing technology too, especially in aseptic processing lines, Alwis (1992). Probably the most successful design, ohmic steriliser APV (European Patent no. 0 032 840 - 1981), suitable for thermal treatment of heterogeneous foods, fruits, cereals, meat mixtures, etc., is shown in Fig.1. Typical application is pasteurisation acidic food products at 90°C and sterilisation of low acidic products at 140°C, see Sastry (1992).

Problems of fouling encountered at the continuous direct ohmic heating are caused by overheating of processed substance in the vicinity of electrodes. Different measures are being suggested to improve performance of the continuous ohmic heater, e.g. mechanical cleaning by oscillating wipers, Moos (1989). In view of the fact, that the nonuniformity of temperature field is caused by the nonuniform residence time of the heated substance, the following arrangement was suggested, see Fig.2. Liquid enters the top of heater and flows downwards through the two side channels. There is no electrical field there and the liquid is preheated only by warm walls. At the bottom of heater the two parallel streams join and liquid flows upward in a nearly uniform electrical field between two planar electrodes (distance 3.6 cm, voltage 220 V, 50 Hz). One side of each preheating channel is formed by a

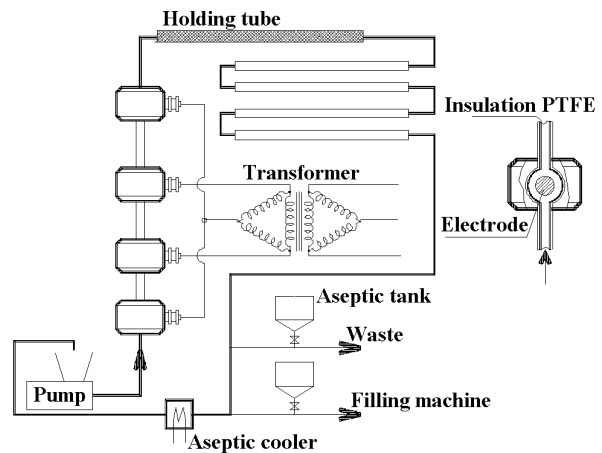
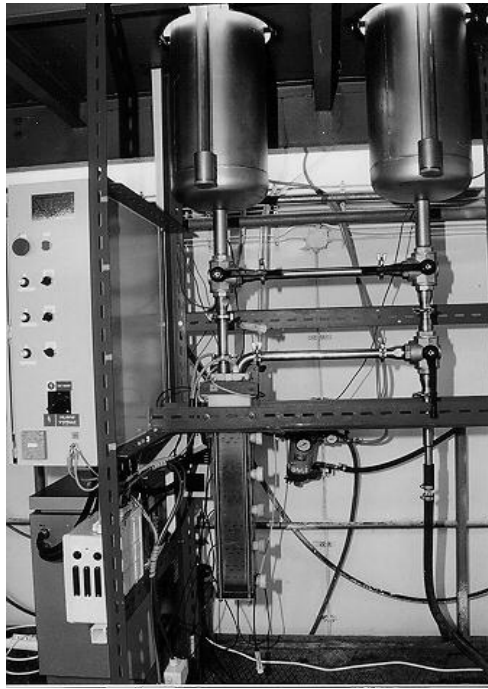


Figure 1 Aseptic heater APV (75-300 kW)



perforated electrode, so a part of cool liquid enters the heating zone sooner than the main stream and it is assumed that this cross-flow displaces overheated liquid, moving slowly along the electrode surface, towards the heating zone center. The effect of perforation on the temperature field is monitored by five Pt100 thermistors located along the centerline of the heating zone, besides other Pt100 located in the inlet and outlet.

Cross-flow through the perforation of electrodes improves also the residence time distribution, i.e. it suppresses the tail of the residence time distribution. The experimental apparatus is equipped by four conductivity probes (at the inlet pipe, at the bottom of the heating vessel and two probes are inside the outlet pipe). Thus it is possible evaluate the RTD characteristics of the heater using stimulus response technique by monitoring responses of the conductivity probes after instantaneous injection of salt solution into the inlet pipe. However, it is not the RTD of the whole apparatus, but the RTD of only the heating zone between electrodes, that is in the center of interest, because residence times in the heating zone have decisive influence on fouling and together with temperature determine the so called F-value - integral thermal effect of sterilisation. It is not possible to measure these residence times directly, but they can be deduced from theoretical models. RTD experiments help to identify unknown parameters of these models, first of all the cross-flow intensity.

The principal tasks of current research are:

1. Optimal design of perforation (and thus the cross-flow) from point of view the RTD characteristics (the RTD should be close to the piston flow in the heating zone).
2. Given the smallest required sterilisation effect (prescribed F-value), the temperature and the fouling at electrodes should be as low as possible.

Simply: An ideal heater is characterized by uniform temperature and uniform residence times in the cross section at the heating zone outlet.

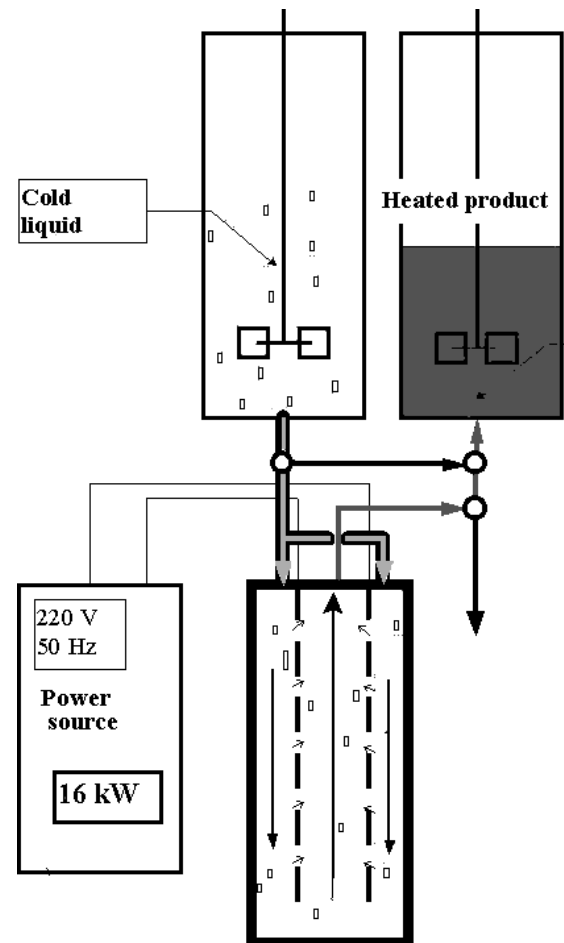


Figure 2 Experimental continuous heater 16 kW

2. Theoretical models

Velocity and temperature fields in the heater are three dimensional, steady and laminar under usual conditions (Re number in the heating channel is typically 200-700 for water or milk and much smaller for majority of supposed food products).

2.1 Integral model - flowrates and 2D approximation of velocity field

Some useful results, e.g., mean calorimetric temperature profiles, can be obtained from integral models based upon assumption of fully developed two dimensional Newtonian velocity profiles, independent of z , as shown in Fig.3. All flowrates will be referred to unit depth of channel (in the z direction). Flowrates in the side channels (\dot{V}_1) and the central channel (\dot{V}_2) decrease with x

$$2\dot{V}_1(x) = \dot{V}_2(x). \quad (1)$$

Their rate of change along the height of channel x is given by the cross-flow through the narrow slots in electrodes

$$\frac{d\dot{V}_1}{dx} = -\dot{V}_{12}, \quad (2)$$

where \dot{V}_{12} is the flowrate from the side channel to the central channel through the unit length of electrode (in the x -direction). Neglecting inertial effects, and assuming $h/H_E \ll 1$, we can approximate the cross flow V_{12} by relationship which holds for fully developed laminar flow between parallel plates

$$\dot{V}_{12}(x) = \frac{p_1(x) - p_2(x)}{12\mu H_E} \cdot \frac{h^3}{l(x)} = \frac{\Delta p(x)}{12\mu H_E} \cdot \frac{h^3}{l_0} \left(1 + \varphi \frac{x}{L}\right) \quad (3)$$

where the last term $1 + \varphi x/L$ describes linear increase of the density of slots ($\varphi=0$ corresponds to the uniform distribution characterized by constant distance l_0 between slots). It follows from Eq.(3) that the permeability of electrodes can be characterized by only one parameter, $\delta = h^3/(12H_2H_E l_0)$.

Gradients of pressure in the x -direction can be expressed in terms of flowrates \dot{V}_1, \dot{V}_2 in the side and central channels, as

$$\frac{dp_1}{dx} = -\frac{12\mu}{H_1^3} \dot{V}_1, \quad \frac{dp_2}{dx} = \frac{24\mu}{H_2^3} \dot{V}_1, \quad \frac{d\Delta p}{dx} = -12\mu \dot{V}_1 \left(\frac{1}{H_1^3} + \frac{2}{H_2^3}\right). \quad (4)$$

Differentiating (4) and using (2,3) we obtain linear differential equation of the second order

$$\frac{d^2 \Delta p}{dx^2} = \frac{h^3}{H_E l_0} \left(\frac{1}{H_1^3} + \frac{2}{H_2^3}\right) \left(1 + \varphi \frac{x}{L}\right) \Delta p \quad (5)$$

that describes difference of pressure between the side channel ($p_1(x)$) and the central channel ($p_2(x)$). Eq.(5) has to be completed by the two following boundary conditions (at the end of electrodes $x=L$, and at the top of heater $x=0$)

$$\Delta p(L) = 0, \quad \frac{d\Delta p}{dx} \Big|_{x=0} = -6\mu \dot{V} \left(\frac{1}{H_1^3} + \frac{2}{H_2^3}\right), \quad (6)$$

where $V = V_2(0) = 2V_1(0)$ is the overall flowrate corresponding to unit depth of channels. Introducing transformed distance x

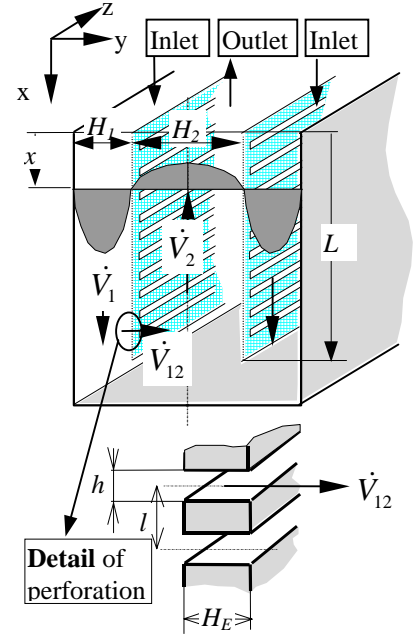


Figure 3 Geometry

$$\xi = \xi_0 \left(1 + \varphi \frac{x}{L}\right), \quad \xi_0 = \sqrt[3]{\frac{h^3 L^2}{\varphi^2 H_E l_0} \left(\frac{1}{H_1^3} + \frac{2}{H_2^3}\right)}, \quad (7)$$

into Eqs.(5,6) we arrive at the final formulation

$$\frac{d^2 \Delta p}{d\xi^2} = \xi \Delta p, \quad \frac{d\Delta p}{d\xi} \Big|_{\xi=\xi_0} = -\frac{6\mu L \dot{V}}{\xi_0 \varphi} \left(\frac{1}{H_1^3} + \frac{2}{H_2^3}\right), \quad \Delta p|_{\xi(L)}=0. \quad (8)$$

An analytical solution of Eq.(8) can be derived using modified Bessel functions of the first kind I_n :

$$\Delta p(\xi) = 12\mu \dot{V} \frac{H_E l_0 \xi_0^2 \varphi}{h^3 L} D \sqrt{\xi} (I_{1/3}^{(L)} I_{-1/3}^{(x)} - I_{-1/3}^{(L)} I_{1/3}^{(x)}) \quad (9)$$

where

$$I_n^{(x)} = I_n\left(\frac{2}{3}\xi^{3/2}\right), \quad I_n^{(L)} = I_n\left(\frac{2}{3}\xi_L^{3/2}\right), \quad I_n^{(0)} = I_n\left(\frac{2}{3}\xi_0^{3/2}\right), \quad (10)$$

and the dimensionless constant D is given by

$$D = \frac{2\sqrt{\xi_0}}{I_{1/3}^{(0)} I_{-1/3}^{(L)} - I_{1/3}^{(L)} I_{-1/3}^{(0)} + \xi_0^{3/2} [I_{-1/3}^{(L)} (I_{4/3}^{(0)} + I_{-2/3}^{(0)}) - I_{1/3}^{(L)} (I_{-4/3}^{(0)} + I_{2/3}^{(0)})]}. \quad (11)$$

Substituting pressure profile (9) into Eq.(4), the following expression describing the flowrate at a given distance from the inlet can be derived as

$$\dot{V}_1(\xi) = \frac{\dot{V}}{2} [1 - g(\xi)], \quad g(\xi) = D [\xi (I_{2/3}^{(x)} I_{1/3}^{(L)} - I_{-2/3}^{(x)} I_{-1/3}^{(L)}) - \xi_0 (I_{2/3}^{(0)} I_{1/3}^{(L)} - I_{-2/3}^{(0)} I_{-1/3}^{(L)})]. \quad (12)$$

Note, that the cross-flow is **independent of viscosity** - it was the main goal of the heater design.

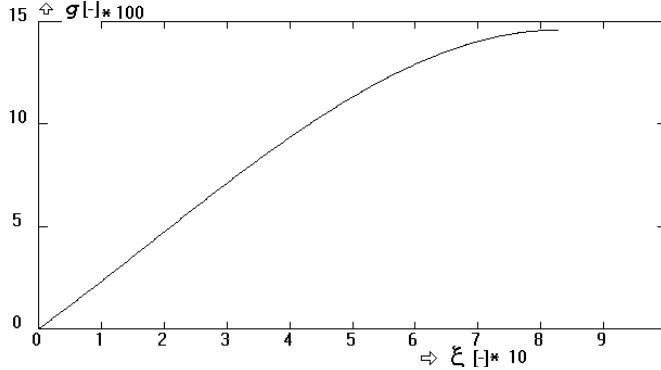


Figure 4 Cross-flow $g(\xi)$ ggStreamlines

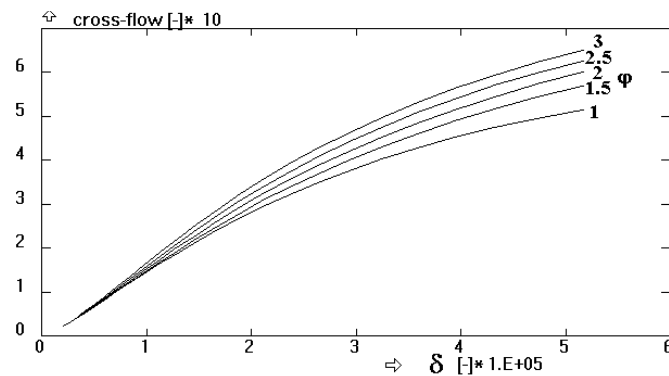


Figure 5 Cross-flow $g_L(\delta, \varphi)$ ggStreamlines

Typical course of $g(\xi)$ calculated for $H_1=0.019$ m, $H_2=0.036$ m, $H_E=0.002$ m, $h=0.0012$ m, $l_0=0.12$ m, $\varphi=2$, and $L=0.6$ m is presented in Fig.4. Function $g(\xi)$ in (12) is the relative amount of cross-flow through the part of electrode from the entry up to the distance ξ and $g(\xi_L)$ is therefore the ratio of flowrate through the whole surface of electrodes and the inlet/outlet flowrate. The relative entrainment $g(\xi_L)$ depends only on two dimensionless parameters, φ , and

$$\delta = \frac{h^3}{12H_E l_0 H_2}.$$

Relationship between relative cross-flow and δ is shown in Fig.5, for $\varphi=1, \dots, 3$. It follows from the graph that, e.g., for $\delta=2 \cdot 10^{-5}$, $\varphi=2$, approximately 30% of liquid flows through electrodes. The value $\delta=2 \cdot 10^{-5}$ was found to be an optimum as will be shown later.

2.2 Residence time distribution

Eq.(12) is the most important result of analysis. It assumes creeping flow, and in this region the transversal velocity profiles can be approximated by parabolic functions

$$u_i(\xi, y) = \frac{6\dot{V}_i(\xi)}{H_i^3} y(H_i - y), \text{ for } i=1,2 \quad (13)$$

where the Cartesian coordinate y is the distance from electrode. Having known velocity field (13) we can calculate streamlines, residence time distribution and also the temperature field.

Streamlines can be expressed using dimensionless stream function ψ which is equal zero for $y=0$ (at electrode) and $\psi=1/2$ at the central channel axis ($y=H_2/2$) and at the wall of vessel ($y=-H_1$), see Fig.6.

$$\psi = \frac{g(\xi)}{2} + (1 - g(\xi)) \left[3\left(\frac{y}{H_2}\right)^2 - 2\left(\frac{y}{H_2}\right)^3 \right] \quad \text{for } y > 0, \text{ and}$$

$$\psi = \frac{g(\xi)}{2} + (1 - g(\xi)) \left[3\left(\frac{y}{2H_1}\right)^2 + 2\left(\frac{y}{2H_1}\right)^3 \right] \quad \text{for } y < 0 \text{ (side channel)} \quad (14)$$

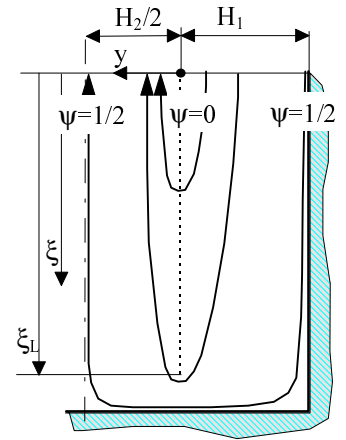


Figure 6 Streamlines

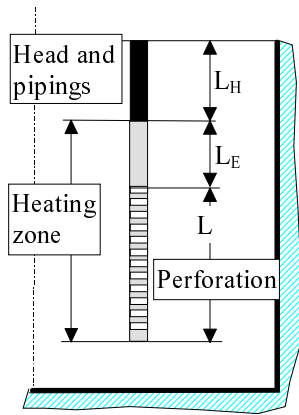


Figure 7 RTD-geometry

Residence times can be calculated by integration of time along streamlines (14), and in this way it is possible to evaluate the residence time distribution $E(t)$ of the whole vessel (side+central channel) and also the RTD of only the heating zone (central channel). Unfortunately the $E(t)$ function cannot be expressed in an analytical form and what is more important the approximation of velocity field describes neither the region under the electrode at the bottom, nor the inlet and outlet pipings (they are rather complicated, like the channels in a head of a combustion engine). In the following graphs the RTD of these parts of heater are substituted by the convective flow between parallel plates, see Fig.7. $E(t)$ courses usually exhibit two peaks, corresponding to the

part of liquid which passes through perforation and to the main stream, see Fig.8. This graph corresponds to the actual geometry of heater (except the perforation, which is not continuous in the real heater): $H_1=0.019$ m, $H_2=0.036$ m, $H_E=0.002$ m, $h=0.001$ m, $l_0=0.12$ m, $\phi=2$, $L=0.6$ m, $L_H=0.2$ m, $L_E=0.1$ m. Though the effect of perforation is clearly seen from the $E(t)$ shape, it is not easy expressed in a quantitative way. As a standard criterion, the $E(t)$ variance σ^2 (second central moment) is usually used: the smaller σ^2 , the sharper is the $E(t)$, and the smaller is the dangerous tail (our effort is oriented on the tail suppression). However, neglecting molecular diffusion, the variance σ^2 is infinitely large in any laminar flow, no matter geometry or configuration of apparatus (an explanation is that in laminar flows tails are always significant).

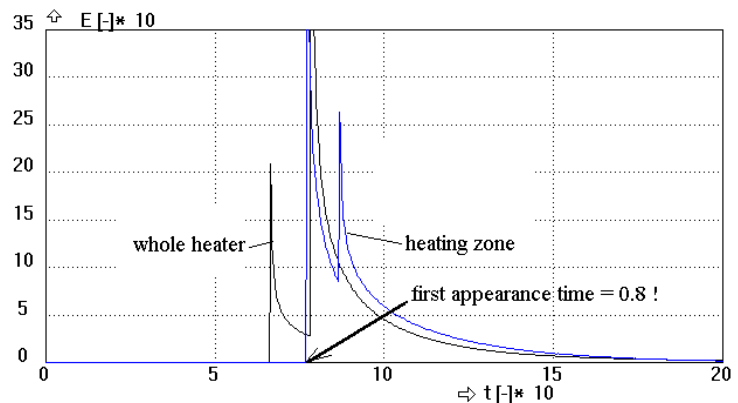


Figure 8 RTD-prediction $E(t)$

This problem cannot be solved quite satisfactory; some information can be obtained by using either cut-off or weighted moments:

$$\sigma^2(s, t_c) = \int_0^{t_c} (t - \bar{t})^2 E(t) e^{-st/\bar{t}} dt \quad (15)$$

(we have used the upper integration limit t_c three times larger than the mean residence time, and $s=0$ for the "optimal" perforation design), see Fig.9.

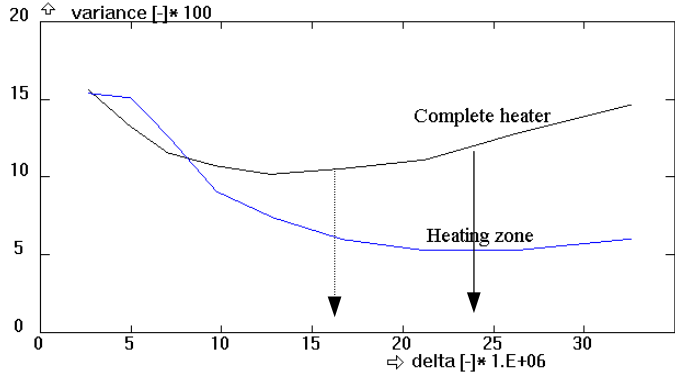


Figure 9 Dimensionless variance $\sigma^2(\delta)$ of $E(t)$

The time of the first appearance of a tracer t_f represents another possibility how to estimate the performance of perforation. The first appearance time concerns the fastest particle of liquid flowing through an apparatus. For example a liquid particle at an axis of circular tube has dimensionless passing time $t_f=1/2$ (assuming fully developed parabolic velocity profile, where $u_{max}=2u$) while the fastest particle flowing between two parallel plates has the first appearance time larger $t_f=2/3$ (it holds $u_{max}=1.5u$ in this case). It is obvious, that dimensionless t_f cannot be greater than 1 (it would have been an ideal piston flow). The value $t_f \cong 0.8$ achieved in the heating zone of the analyzed configuration is excellent, but cannot be verified experimentally; the only measurable value is the first appearance time of the whole heater, Fig.10. Conclusions:

It seems, that an optimum of perforation (permeability of electrodes) expressed in terms of δ , exists, because for $\delta=2.1 \cdot 10^{-5}$ the maximum of the first appearance time and at the same time a minimum of the $E(t)$ variance is achieved. However, this optimum differs from the optimum observed from outside, which predicts slightly lower value of δ .

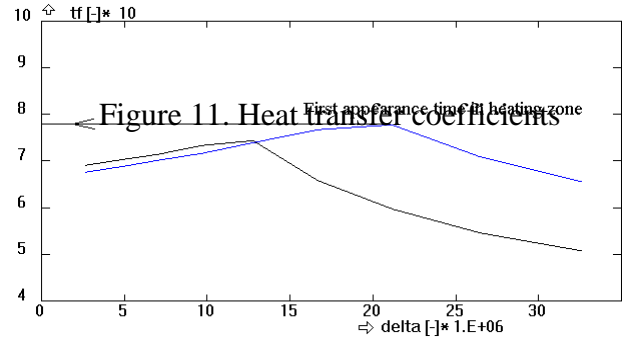


Figure 10. First appearance time $t_f(\delta)$

2.3 Integral model - temperature field

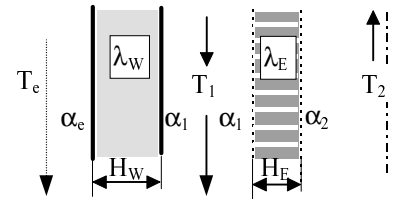
An approximation of temperature profiles along the side (T_1) and the central channel (T_2) can be described by integral balances of enthalpy flows:

$$\rho c_p \dot{V}_1 \frac{dT_1}{dx} = k_E (T_2 - T_1) - k_e (T_1 - T_e), \quad (\text{side channel}) \quad (15)$$

$$\rho c_p \dot{V}_2 \frac{dT_2}{dx} = 2(\rho c_p \frac{d\dot{V}_1}{dx} - k_E)(T_1 - T_2) - (\kappa_0 + \kappa_1 T_2) \frac{U^2}{H_2} \quad (\text{central channel}) \quad (16)$$

where k_E , k_e are heat transfer coefficients describing heat transfer through electrode and through the outer wall, respectively, see Fig.11:

$$k_E = \frac{1}{\frac{1}{\alpha_1} + \frac{1}{\alpha_2} + \frac{H_E}{\lambda_E}}, \quad k_e = \frac{1}{\frac{1}{\alpha_1} + \frac{1}{\alpha_e} + \frac{H_W}{\lambda_W}} \quad (17)$$



The last term in Eq.(16) represents the volumetric source of electric heat, U is voltage (difference of electric potential between electrodes) and $\kappa = \kappa_0 + \kappa_1 T_2$ is the specific electrical conductivity of heated substance, linearly increasing with temperature T . This temperature

dependency cannot be neglected, as most substances increase the conductivity twice when the temperature is increased by about 50°C.

Subtracting Eq.(16), (17) and rearranging terms we obtain

$$\rho c_p \frac{d}{dx} [\dot{V}_2 (T_2 - T_1)] = -(\kappa_0 + \kappa_1 T_2) \frac{U^2}{H_2} - 2k_e (T_e - T_1). \quad (18)$$

Any two of three equations (15,16,18) together with the boundary conditions

$$T_1(L)=T_2(L), \quad \text{and} \quad T_1(0)=T_0 \quad (19)$$

represent unique description of the mean temperature profiles. All the equations are linear, suggesting possible analytical solution, nevertheless it would be very difficult due to the complicated form of $\dot{V}_2 = \dot{V}(1 - g(\xi))$, and it is much more easier to find the solution numerically.

Eqs. (15,18) can be rearranged introducing dimensionless distance $\xi = \xi_0(1 + \phi x/L)$ and the temperature difference $\Delta T = T_2 - T_1$

$$\xi_0 \frac{d}{d\xi} [(1 - g(\xi)) \Delta T] = -\frac{\kappa_0 + \kappa_1 (T_1 + \Delta T)}{K} - \frac{T_e - T_1}{Pe_e}, \quad (20)$$

$$\xi_0 (1 - g(\xi)) \frac{dT_1}{d\xi} = \frac{\Delta T}{Pe_E} - \frac{T_1 - T_e}{Pe_e}, \quad (21)$$

where

$$K = \frac{\rho c_p \phi \dot{V} H_2}{U^2 L}, \quad Pe_e = \frac{\rho c_p \phi \dot{V}}{2k_e L}, \quad Pe_E = \frac{\rho c_p \phi \dot{V}}{2k_E L}. \quad (22)$$

Solution of these equations for the following set of parameters: $U=220$ V, $\kappa_0=0.024$ S.m⁻¹, $\kappa_1=0.0008$ S.m⁻¹.K⁻¹, $\rho=1000$ kg.m⁻³, $c_p=4200$ J.kg⁻¹.K⁻¹, $k_e=6.43$ W.m⁻².K⁻¹, $k_E=200$ W.m⁻².K⁻¹, $\phi=2$, $H_2=0.036$ m, $L=0.6$, $V=3.75 \cdot 10^{-4}$ m².s⁻¹, giving dimensionless parameters $K=0.0039$, $Pe_E=13$, $Pe_e=408$, is presented in Figs.12,13. The four temperature profiles, denoted by parameter K, correspond to different flowrates. It is obvious that the higher is flowrate (or smaller K), the lower is the temperature increase. What is not so obvious: the higher is cross-flow, the higher is the temperature increase and the power of heater (at the same flowrate and voltage). Temperature profiles, corresponding to the suppressed cross-flow case ($\delta=0$) increase rapidly towards the outlet (not shown in figs.), while for excessively high cross-flow (e.g. $\delta=3.3 \cdot 10^{-5}$) the temperatures rise much faster at the bottom and this increase slows down towards the outlet, see Fig.13. There exists an optimal level of cross-flow, giving almost linear courses of temperature, see Fig.12 calculated for $\delta=10^{-5}$.

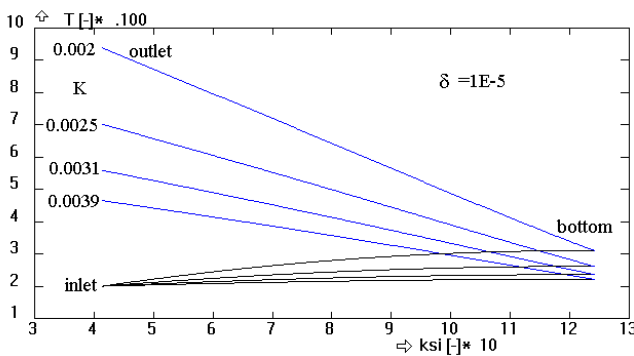


Figure 12 Temperature profiles at low $\delta=10^{-5}$

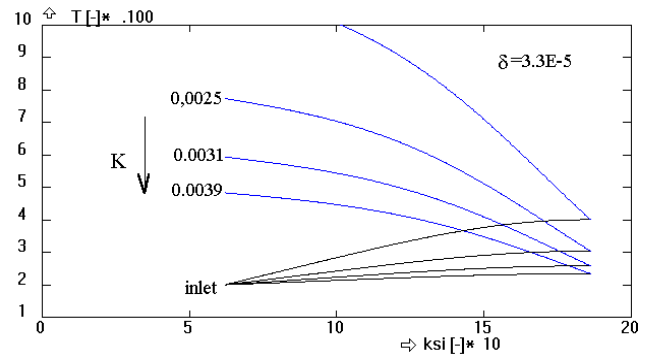


Figure 13 Temperature profiles at high $\delta=3.3 \cdot 10^{-5}$

3. Experiments

All presented results were obtained from measurements with tap water as a model liquid. Although the apparatus is equipped by electronic monitoring of liquid level in the storage tank, the flowrate was evaluated by weighing the mass of water at a certain time measured by stopwatch.

3.1 Velocity field - visualization, ultrasonic monitoring, numerical modeling

The heating section is made from transparent material (Lexan) and thus it is possible to observe the flowfield visually, using coloured tracer (water solution of potassium permanganate) injected into the inlet pipe. This simple experiment revealed one important drawback of the current version of electrodes: Formation of small closed vortices behind the liquid jets streaming from the holes in electrodes at higher flowrates, see Fig.14. This

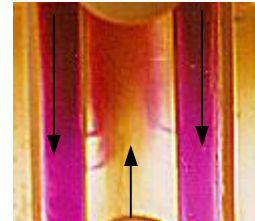


Fig.14

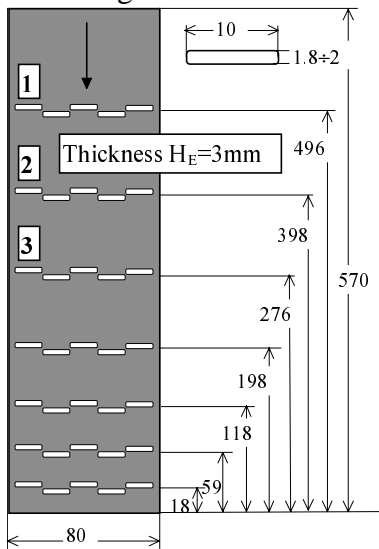


Figure 15 Geometry of perforated electrode

Fig.16.

The Fluent predicts relative cross-flow of about 40%, while the integral model gives more than 70%! The last value is obviously overestimated, because slots were too wide and assumptions of integral model cannot hold. The squares in Fig.16 are experimental results obtained by measurement of axial velocity profiles using Ultrasonic Velocity Profile Monitor X-2-PS DANTEC MT, equipped with the 4MHz probe. This probe was fixed on a adjustable support and inserted into the heater near its bottom. This measurement was not very accurate, as the velocities of liquid were too small (2-3 cm/s), and a noise and reflection of sound waves from walls and electrodes invalidate most data points (indicated as zero velocity), so that rather laborious (and questionable) data postprocessing had to be done. By the UVP-Monitor a typical operational range of flowrates from 30 to 60 ml.s⁻¹ had been investigated, but only the data for 45 ml.s⁻¹, corresponding to the numerical simulation by Fluent, are shown in Fig.16.

phenomenon could have been expected, and a special geometry, characterized by inclined slots in electrodes was initially suggested (however, only the perpendicular slots were manufactured for simplicity, and what is more important, instead of the specified width of slots $h=0.001$ mm, the actual value was nearly two times higher, giving very large value of $\delta=4.5 \cdot 10^{-5}$, which is outside the design range considered in the previous paragraphs). The existence of swirling regions was confirmed also numerically using Fluent 5, for the geometry of electrodes in Fig.15 (all numbers are in mm). This numerical model (comprising side channels, bottom and the central channel) was three-dimensional, and even if the symmetry was utilized, a very large number of computational cell, 380000, was necessary to achieve acceptable accuracy (automatic refining of unstructured mesh was used). The same case was calculated according to Eq.(12) and resulting axial profile of \dot{V}_2 is in

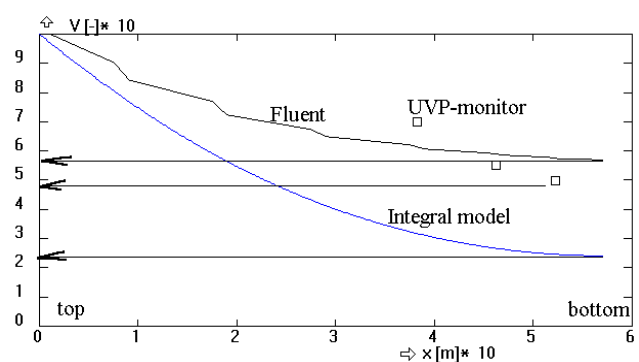
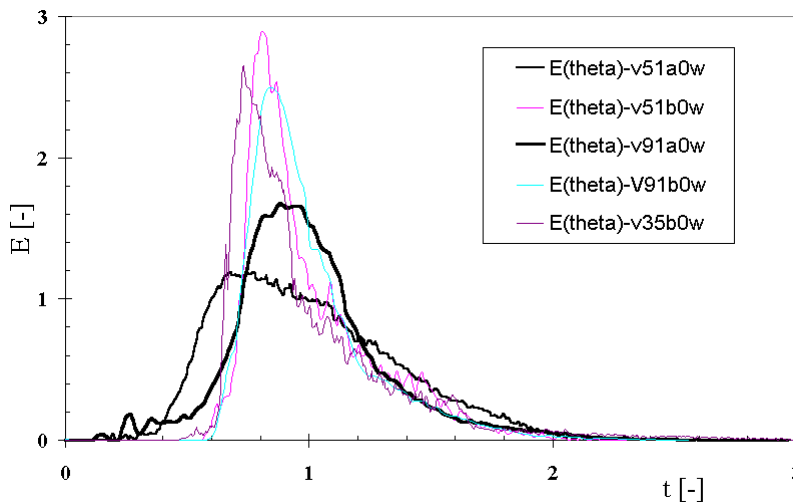


Figure 16 Relative cross-flow

3.2 Residence time distribution

Residence time distribution was investigated by the stimulus response method, using conductivity probes located at the inlet and outlet of the ohmic heater. Saturated solution of NaCl manually injected into the inlet (5 ml, 2 seconds) was used as a tracer. Examples of normalized impulse responses ($E(t)$) are presented in Fig.17 for different flowrates and different configuration of perforation (some holes were masked by plastic tape).

Configuration	diml. Variance - probe #3			diml. Variance - probe #4		
	min	max	average	min	max	average
A0 - all holes open	0.1030	0.1210	0.1113			
	0.1240	0.1340	0.1268	0.1170	0.1310	0.1254
C2 - 2 rows closed	0.0710	0.0740	0.0720	0.0700	0.0710	0.0703
	0.0700	0.0740	0.0723	0.0680	0.0720	0.0703
	0.0780	0.0860	0.0836	0.0740	0.0840	0.0786
C3 - 3 rows closed	0.0630	0.0680	0.0657	0.0670	0.0740	0.0693
	0.0650	0.0900	0.0737	0.0640	0.0860	0.0740
	0.0470	0.0510	0.0490	0.0500	0.0520	0.0510
	0.0720	0.0810	0.0775	0.0800	0.0880	0.0835
	0.0720	0.0850	0.0797	0.0740	0.0840	0.0773
C4 - 4 rows closed	0.0570	0.0770	0.0670	0.0560	0.0800	0.0667
	0.0550	0.0580	0.0563	0.0490	0.0580	0.0550
B0- all holes closed	0.0570	0.0700	0.0648	0.0610	0.0810	0.0680
	0.0630	0.0920	0.0742	0.0630	0.1050	0.0846
	0.1190	0.2270	0.1588	0.1530	0.2100	0.1850



Recorded data were processed in the same way as previously by using variances calculated from Eq. (15), some results are in the table above. It seems that neither the configuration when all slots in the electrode are opened, nor the case when all the holes are closed is optimum. The smallest variance was observed when only the first three rows of slots were masked. It is well known that the RTD measurement in laminar flow

Figure 17 Impulse responses for flowrates 30, 50 and 90 ml/s

is rather difficult and that the calculated variances are not very reliable. Even if we admit significant experimental errors caused, e.g., by the imperfect injection of tracer (only one needle was used and we did not take any special measure ensuring the proper homogenization of tracer after injection), the results confirm, that the current design of perforation will have to be changed, and the width of slots should be reduced.

3.3 Temperature profiles

Temperatures in the ohmic heater are measured by Pt100 thermometers and together with the actual electric power are recorded by PC. Fig. 18 shows results, obtained when using homogeneous stainless steel electrodes. Fig. 19 corresponds to the same conditions, but with composite electrodes, which have electrically insulated outer face (by an epoxy layer). The aim of this modification is elimination of electrical field in the side channels and suppression excessive electrical preheating.

Important temperatures are "head in", "head out", "T1" and "T5". The "head in" temperature is measured at the inlet channel when the heated media incomes into the heating bath. The "T1" temperature is measured at the bottom of the bath (between electrodes) and "T5" is measured at the top of the heating section (at the end of electrodes). Temperatures "T2", "T3" and "T4" are measured between these two. The temperature "head out" is measured at the outlet channel, when the heating process is finished.

Let us look for important temperature differences. First one is between "head-in" and "T1". This difference is given by pre-heating effect (cooling electrodes). The second is between "T1" and "T5" and is given by ohmic heating process intensity. Difference between "T5" and "head-out" is important, because it shows effect of temperature smoothing after the heating process is finished. The line "theory" shows the value of temperature which is given by calorimetric equation for given power, thermal capacity and flowrate.

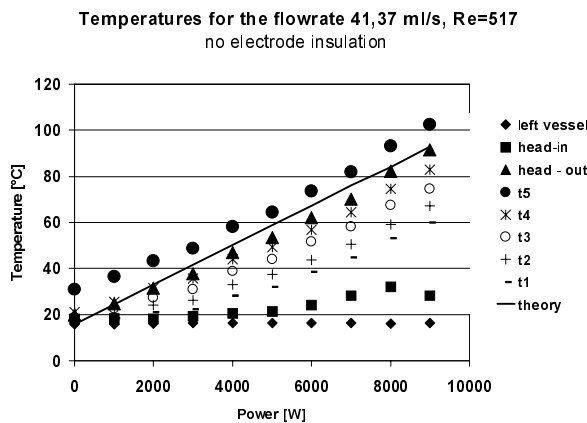


Figure 18. Temperature profiles dependency on electric power. No outer electrical insulation.

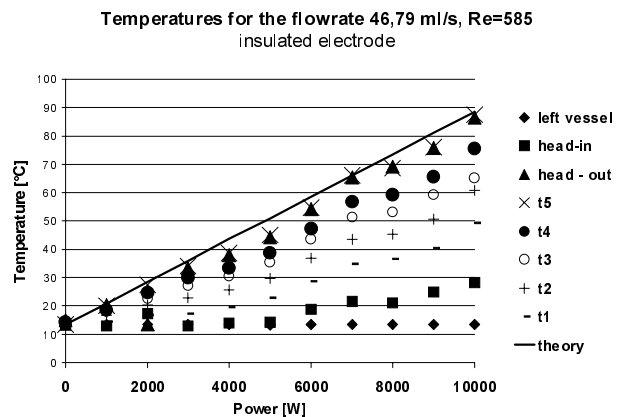


Figure 19. Relationship between temperatures and heating power. Electrical insulation of electrodes in the side channels.

4. Conclusions :

All the presented experimental results are preliminary and serve only for tuning the optimal design of electrodes. Current research is oriented on fouling and heating non-Newtonian liquids.

Authors thank National Agency for Agricultural Research of Czech Republic for supporting this project.

List of important symbols

c_p	specific heat capacity	[J.kg ⁻¹ .K ⁻¹]
$E(t)$	residence time distribution (impulse response)	[-]
$g(\xi)$	relative flowrate through perforation (from the top of heater up to the distance ξ)	[-]
h	width of slot	[m]
H_E	thickness of electrode	[m]
H_1	width of side channel	[m]
H_2	width of central channel (distance between plate electrodes)	[m]
L	length of electrode	[m]
l_0	initial distance between slots	[m]

$p_1(\xi)$	pressure in the side channel	[Pa]
$p_2(\xi)$	pressure in the central channel (in the heating zone)	[Pa]
$\Delta p = p_1 - p_2$	pressure drop across electrode	[Pa]
t	dimensionless residence time (time related to the mean residence time)	[-]
T_1, T_2	mean calorimetric temperatures in the side and in the central channel	[K]
\dot{V}	flowrate related to the unit depth of channels (actual flowrate divided by width of electrode)	$[\text{m}^2 \cdot \text{s}^{-1}]$
$\dot{V}_1(\xi), \dot{V}_2(\xi)$	flowrate in the side (1) and the central (2) channels	$[\text{m}^2 \cdot \text{s}^{-1}]$
x	axial distance measured from the top of heater	[m]
y	distance from electrode	[m]
α_e	heat transfer coefficient at the outer surface of heater	$[\text{W} \cdot \text{m}^{-2} \cdot \text{K}^{-1}]$
α_i	heat transfer coefficient inside the side and the central channel	$[\text{W} \cdot \text{m}^{-2} \cdot \text{K}^{-1}]$
$\delta = h^3 / (12H_{E1}H_2)$	dimensionless hydraulic permeability of electrodes	[-]
ϕ	nonuniformity of perforation	[-]
κ_0	specific electrical conductivity	$[\text{S} \cdot \text{m}^{-1}]$
λ	thermal conductivity	$[\text{W} \cdot \text{m}^{-1} \cdot \text{K}^{-1}]$
μ	viscosity	[Pa.s]
ρ	density	$[\text{kg} \cdot \text{m}^{-3}]$
σ^2	variance (second central moment of normalised impulse response)	[-]
$\xi = \xi_0(1 + \phi x/L)$	dimensionless distance from the top of heater	[-]

References

1. de Alwis A.A.P., Fryer P.J.: The use of direct resistance heating in the food industry, *Journal of Food Engineering*, Vol. 15, 1992, pp. 21-48
2. Hauser, J, Y.: Temperature Control in an Ohmic Process, *International Application PCT*, no. WO 93/04421, 1993
3. Moos, R.F.: Apparatus for heating electrically conductive flowable media and methods of use of such apparatus, *International Application PCT* no. WO 89/00384, 1989
4. Metaxas A.C.: *Foundations of Electroheat*, J.Wiley&Sons, Chichester, 1996
5. Palmieri, L. et.al.: Residence time distribution of food suspensions containing large particles when flowing in tubular systems. *Journal of Food Engineering*, 17, No.3, 1992, s.225-239
6. Sastry, K.S.: A Model for Heating of Liquid-Particle Mixtures in a Continuous Flow Ohmic Heater, *Journal of Food Process Engineering*, Vol. 15, pp. 263-278, 1992
7. Simpson, D. P.: Apparatus for Heating Electrically Conductive Flowable Media, *European Patent Application* no. 0 032 840, 1981
8. Simpson, D.P.: Ohmic heater including electrodes arranged along a flow axis to reduce leakage current, *US Patent* no.5,440,667; 1995
9. Stirling, R.: Surface Fouling Resistant Materials, *International Application PCT*, no. WO 90/147 40, 1990
10. Zhang, L.; Fryer, P.J.: Food sterilization by Electrical Heating: Sensitivity to Process Parameters, *AIChE Journal*, Vol. 40, No. 5, pp. 888-898, May 1994
11. Zhang, L.; Fryer, P. J.: Models for the Electrical Heating of Solid-liquid Food Mixtures, *Chemical Engineering Science*, Vol. 48, No. 4, pp. 633-642, 1993
12. Žitný, R.; Šesták, J.: Direct Ohmic Heating in laminar flows in ducts, *Acta Polytechnica*, Vol.26, 1996, pp. 71-83